Reversible Chemisorption of Sulfur Dioxide in a Spin Crossover Porous Coordination Polymer

Zulema Arcís-Castillo,[†] Francisco J. Muñoz-Lara,[†] M. Carmen Muñoz,[‡] Daniel Aravena,[§] Ana B. Gaspar,[†] Juan F. Sánchez-Royo,[||] Eliseo Ruiz,[§] Masaaki Ohba,[⊥] Ryotaro Matsuda,[#] Susumu Kitagawa,[#,∇] and José A. Real*,[†]

[†]Instituto de Ciencia Molecular (ICMol), Universidad de Valencia, 46980 Paterna, Valencia, Spain

[‡]Departamento de Física Aplicada, Universitat Politècnica de València, E-46022 Valencia, Spain

[§]Departament de Química Inorgànica and Institut de Recerca de Química Teòrica i Computacional, Universitat de Barcelona, Barcelona 08028, Spain

[||]Instituto de Ciencia de los Materiales, Universidad de Valencia, 46100 Burjassot, Valencia, Spain

[⊥]Department of Chemistry, Faculty of Science, Kyushu University, Hakozaki, Higashi-ku, Fukuoka 812-8581, Japan

[#]Institute for Integrated Cell-Material Sciences (iCeMS), Kyoto University, Yoshida, Sakyo-ku, Kyoto 606-8501, Japan

[∇]ERATO Kitagawa Integrated Pores Project, Japan Science and Technology Agency (JST), Kyoto Research Park, Shimogyo-ku, Kyoto 600-8815, Japan

Ⓢ *Supporting Information*

ABSTRACT: The chemisorption of sulfur dioxide (SO_2) on the Hofmann-like spin crossover porous coordination polymer (SCO-PCP) $\{Fe(pz)[Pt(CN)_4]\}$ has been investigated at room temperature. Thermal analysis and adsorption−desorption isotherms showed that ca. 1 mol of SO_2 per mol of $\{Fe(pz)[Pt(CN)_4]\}$ was retained in the pores. Nevertheless, the SO_2 was loosely attached to the walls of the host network and completely released in 24 h at 298 K. Single crystals of $\{Fe(pz)[Pt(CN)_4]\} \cdot nSO_2$ ($n \approx 0.25$) were grown in water solutions saturated with SO_2, and its crystal structure was analyzed at 120 K. The SO_2 molecule is coordinated to the Pt^{II} ion through the sulfur atom ion, Pt−S = 2.585(4) Å. This coordination slightly stabilizes the low-spin state of the Fe^{II} ions shifting the critical temperatures of the spin transition by 8−12 K. DFT calculations have been performed to rationalize these observations.

SO₂ Capture
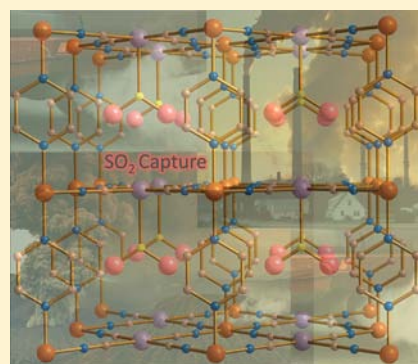
INTRODUCTION

Natural and anthropogenic release of sulfur dioxide into our environment is an issue of global concern.[1] Sulfur dioxide is a main intermediate in the oxidation cycle of sulfur compounds, which is further oxidized in the atmosphere to produce smog and acid rain.[2] This has created a great deal of research focused on removing SO_2 from emissions of combustion sources. Consequently, several approaches including the use of microporous activated carbons,[3] zeolites,[4] metallic oxides,[5] and metal complexes,[6] as well as metal surfaces,[7] have been proposed as efficient models for storing and/or transforming SO_2.

Porous coordination polymers (PCPs), also called porous metal−organic frameworks (PMOFs), are a new class of porous materials with highly regular designable and flexible pores and large internal surface areas.[8] These attributes have attracted a great deal of interest as alternative adsorbents.[9] However, very few studies regarding PCPs have specifically been focused on the study of SO_2 adsorption. As far as we know, efficiency of SO_2 adsorption has only been investigated on Prussian blue

analogues formulated $M_3[Co(CN)_6]_2 \cdot nH_2O$ (M = Co, Zn)[10] and a series of poly-carboxylate-based compounds.[11,12]

Hofmann clathrates are an alternative class of well-known PCPs.[13] In particular, Hofmann-type PCPs with formula $\{Fe(pz)[M^{II}(CN)_4]\}$ (pz = pyrazine, M^{II} = Ni, Pd, Pt) represent a singular class of bistable chemo-responsive Fe^{II} spin crossover (SCO) materials switchable between the paramagnetic (yellow-orange) high-spin (HS) state and the diamagnetic (deep-red) low-spin (LS) state through guest adsorption processes at room temperature.[14] Physisorption of O_2, N_2, or CO_2 has no effect on the spin state of these SCO-PCPs, while common hydroxylic solvents and five- and six-membered aromatic rings stabilize the HS state. In contrast, physisorption of CS_2 and CH_3CN (M^{II} = Ni) stabilizes the LS state. These reversible chemo-induced spin-state changes feature a memory effect which takes place inside the thermal hysteresis loop characteristic of the SCO of $\{Fe(pz)-[M^{II}(CN)_4]\}$. Furthermore, irreversible chemisorption of

halogens occurs at the M^{II} = Pt sites with remarkable influence on the critical temperatures without affecting the cooperativity of the SCO. The oxidative addition of Br_2 and I_2 to Pt^{II} stabilizes the LS state while Cl_2 stabilizes the HS state.

On the basis of these results and inspired by the reversible crystalline-state reaction of gaseous SO_2 with nonporous crystalline materials consisting of square-planar organoplatinum molecules previously reported,[6] we decided to investigate the adsorption of gaseous SO_2 in $\{Fe(pz)[Pt^{II}(CN)_4]\}$ (**1**). Here we report the reversible binding of SO_2 to the coordinatively unsaturated Pt^{II} sites of **1** and its influence on the spin state of the Fe^{II} in $\{Fe(pz)[Pt(CN)_4]\}$. DFT calculations have also been applied in order to justify the observed results.

RESULTS AND DISCUSSION

Thermal Stability and Adsorption–Desorption Isotherms. Microcrystalline samples of $\{Fe(pz)[Pt^{II}(CN)_4]\}\cdot SO_2$ (**1·1SO₂**) were obtained from **1**[14b] deposited in vials placed in sealed flasks connected to a pressurized SO_2 cylinder. The parent compound **1** displays a rather abrupt SCO behavior with thermal hysteresis centered at room temperature being the critical temperatures $T_c^{down} \approx 285$ K (cooling mode) and $T_c^{up} \approx 309$ K (heating mode). Below T_c^{down}, in the cooling branch of the hysteresis, the thermodynamically stable state is the LS, and the solid gets a deep-red color, while above this temperature the HS state is stable and the solid becomes yellow-orange. The same holds for T_c^{up} in the heating branch of the hysteresis.[14b] Interestingly, adsorption of $SO_2(g)$ induces an upward shift of the critical temperatures of the resulting clathrate **1·1SO₂** (see Magnetic Properties section). Thus, exposure of **1** to $SO_2(g)$ for a few minutes at $T = 291$ K induces a change from yellow-orange to deep-red suggesting a change of the Fe^{II} ground state from the HS state to the LS state upon SO_2 adsorption. However, at temperatures above 297 K, the adsorption of SO_2 induces a tenuous change of color to ocher suggesting that adsorption of SO_2 takes place without change of spin state (see Magnetic Properties section) (Figure S1, Supporting Information).

The thermal analysis shows that **1** adsorbs ca. 1 mol of SO_2 per mol of compound. The SO_2 is desorbed in the temperature interval 298−400 K (see Figure 1a). The two subsequent steps in the thermal decomposition correspond to the weight loss of one pyrazine molecule and 4 CN groups, respectively. The remaining product corresponds quite well to a 50% mixture of metallic Fe and Pt. It is worth mentioning that even at room temperature the molecule of SO_2 is loosely attached to the pores and slowly releases. The loss of SO_2 is practically completed in 24 h at 298 K. This spontaneous desorption process at 298 K fits reasonably well to an exponential process characterized by a velocity constant $k \approx 3.7 \times 10^{-5}$ s^{-1} (Figure 1b).

The adsorption isotherm at 293 K displays a type I behavior featuring a sharp SO_2 uptake at low pressures (below 50 mbar) and practically reaches saturation at 0.20 bar, which corresponds to ca. 1.32 mol of SO_2 per mol of **1** (Figure 2). The desorption isotherm matched the adsorption one after repeated cycles. The same saturation values were obtained at 258 K in a first cycle. However, after vacuuming for 4 h at 258 K, the resulting "**1**" species readsorbed ca. 0.8 mol of SO_2 per mol of compound in a successive cycle showing that, at 258 K, ca. 0.5 mol of SO_2 per mol of compound remain trapped in the pores. It is worth noting that in similar circumstances the Pd^{II} and Ni^{II} analogues exhibited corresponding adsorption isothems
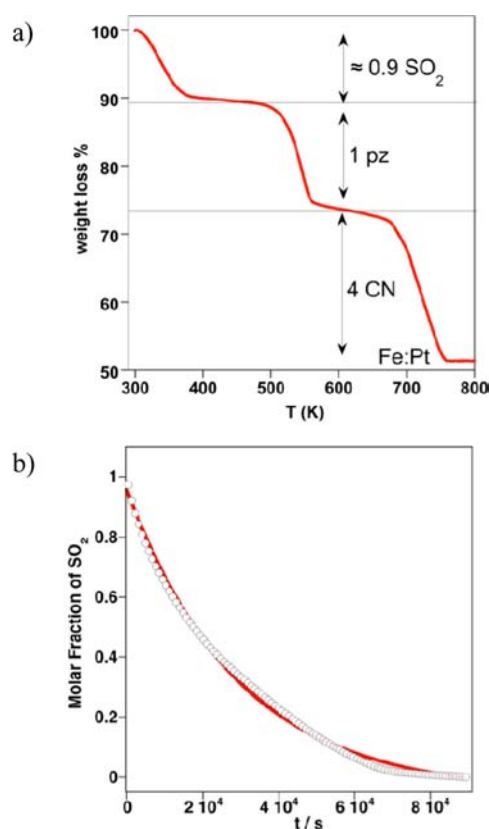

Figure 1. Thermal decomposition (a) and kinetics of the spontaneous desorption of SO_2 at 298 K (b) for **1·nSO₂**.
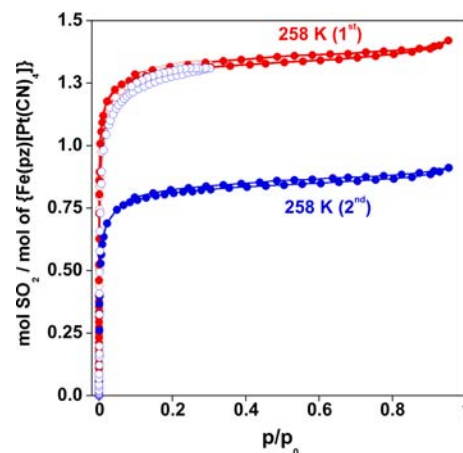

Figure 2. SO_2 sorption−desorption isotherms for **1** at 293 K (○) and at 258 K (●). Red and blue color codes refer to the first and second sorption−desorption cycles, respectively (see text).

with similar saturation value in the first cycle, but the amount of SO_2 trapped decreases significantly (Figure S2, Supporting Information). These results suggest stronger affinity of Pt^{II} to SO_2 than Pd^{II} and Ni^{II}. Nevertheless, **1**, or in general $\{Fe(pz)[M^{II}(CN)_4]\}$, recovered full adsorption capacity at 293 K in all cases. It deserves mention that stabilization of the LS state upon adsorption of SO_2 was only evidenced for the Pt^{II} derivative.

Extrapolation of the adsorbed amount at 1 bar and 293 K gives ca. 1.32 mol per mol of **1** which corresponds to 3.03 mmol g^{-1} (Figure 2). Slightly larger values were obtained for the homologous Pd and Ni derivatives: 1.34 mol/mol (3.87

mmol g^{-1}) and 1.40 mol/mol (4.71 mmol g^{-1}), respectively. This uptake is significantly higher than the values obtained for BPL-activated carbon (0.15 mmol g^{-1}),[5c] CoFe$_2$O$_4$ (0.62 mmol g^{-1}),[5c] MOF74 analogues [0.63 mmol g^{-1} (Co), 1.60 mmol g^{-1} (Mg), 0.04 mmol g^{-1} (Ni), and 0.26 mmol g^{-1} (Zn)],[10] and M$_3$[Co(CN)$_6$]$_2$·nH$_2$O (2.5 mmol g^{-1}),[11] but smaller than the value observed for [Al$_2$(OH)$_2$(C$_{16}$O$_8$H$_6$)] (8 mmol g^{-1}).[12]

Crystal Structure. Single crystals of **1**·nSO$_2$ were prepared from a modification of the slow-diffusion technique previously reported[14b] using sealed H-type vessels filed with saturated solutions of SO$_2$ in water. The crystals were picked directly out from the mother liquor, soaked in Paratone oil, and mounted on the goniometer and measured at 120 K. As expected, the compound crystallizes in the $P4/mmm$ space group forming a three-dimensional pillared layer-type porous framework consisting of cyano-bridged Fe^{II}–Pt^{II} bimetallic layers and interlayer pz bridges.[14b,c] At this temperature the Fe^{II} is in the LS spin state.

The disordered SO$_2$ guest molecule is situated in the middle of the channels just between the Pt^{II} atoms. Indeed, the SO$_2$ molecule axially coordinates the Pt^{II} ions defining a square pyramid [PtN$_4$S] site with a Pt–S bond length 2.585(4) Å. The S–O bond length and O–S–O bond angle were found to be 1.450(5) Å and 114.0(4)°, respectively. Figure 3 shows a view
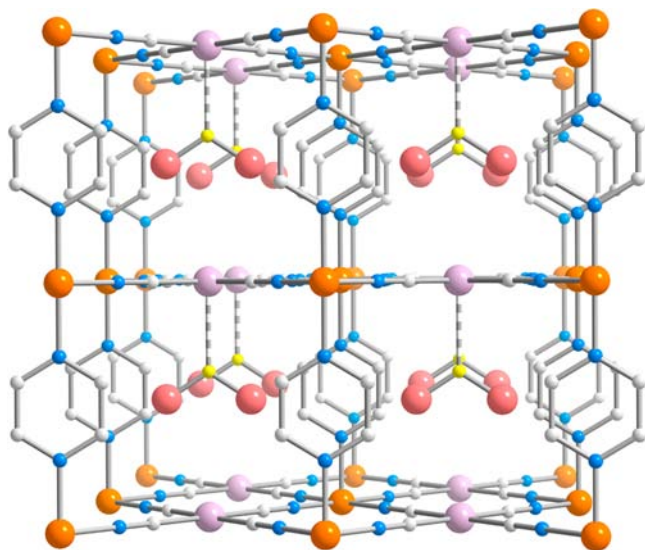

Figure 3. Fragment of the structure of **1**·nSO$_2$. Color code: Fe (orange), Pt (light pink), S (yellow), N (blue), C (gray).

of the framework consistent with an ideal stoichiometry **1**·1SO$_2$ (n = 1). In this picture, one of two possible orthogonal orientations of the pz and SO$_2$ molecules has been removed for sake of clarity (a complete picture is shown in Figure S3, Supporting Information). On the basis of the positional disorder parameters, the actual load of SO$_2$ molecules in the reported crystal structure was estimated to be ca. 25% ($n \approx$ 0.25) per unit cell.

From the total solvent accessible volume, 83 Å^3,[15] a pore volume of 0.115 cm^3 g^{-1} is estimated. This volume is a little smaller than the value 0.133 cm^3 g^{-1} obtained from the amount adsorbed at ca. 1 bar at 293 K (3.03 mmol g^{-1}). To convert mmol g^{-1} to cm^3 g^{-1} we have considered that the density of liquid SO$_2$ at its boiling point is 1.458 g cm^{-3}. The slight

experimentally observed SO$_2$ overload could be ascribed to adsorption on the surface of the crystallites.

Magnetic Properties. Figure 4 compares the product $\chi_M T$ versus T of **1** and a freshly prepared sample of **1**·1SO$_2$ (χ_M is
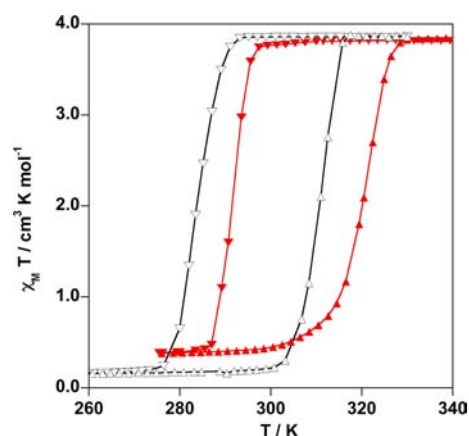

**Figure 4.** Magnetic properties of **1** (black line) and **1**·1SO$_2$ (red line).

the molar magnetic susceptibility, and T is temperature). In order to avoid any significant loss of SO$_2$ during the magnetic measurements, **1** was loaded with SO$_2$ at 305 K in the HS state. Then, the magnetization was immediately measured in the cooling mode from 310 to 270 K at 2 K min^{-1}. At 310 K, $\chi_M T$ is about 3.6–3.8 cm^3 K mol^{-1}, a typical value for an Fe^{II} ion in the HS state (S = 2) featuring strong orbital contribution. The $\chi_M T$ product remains constant upon cooling down to 297 K. Below this temperature, $\chi_M T$ drops to a value about 0.2–0.4 cm^3 K mol^{-1} at ca. 287 K indicating the occurrence of practically complete spin transition from the HS state to the diamagnetic LS state, characterized by a critical temperature $T_c^{down} \approx$ 291 K. As expected, in the heating mode (2 K min^{-1}) the $\chi_M T$ versus T curve does not match that of the cooling mode defining a large thermal hysteresis ca. 29 K wide. The critical temperature for the LS-to-HS transition in the heating mode was estimated to be T_c^{up} = 320 K. Comparison between $\chi_M T$ versus T plots of **1** and **1**·1SO$_2$ denotes a clear upward shift of the critical temperatures of 8–12 K (depending on the sample) which indicates a small but significant stabilization of the LS state in the Fe^{II}. Consequently, comparison between the cooling branches of **1** and **1**·1SO$_2$ denotes the occurrence of a narrow interval of temperatures, ca. 285–291 K, in which adsorption of SO$_2$ induces the switch from the HS state to the LS state. The temperature interval is in this case more marked for the heating branches, 309–320 K. Thus, desorption of SO$_2$ in this interval will induce the reverse switch of spin state.

DFT Calculations. A theoretical study of **1**·1SO$_2$ was carried out using density functional theory as implemented in the Siesta code.[16] The PBESol functional[17] together with a numerical basis set and pseudopotentials were employed[18] (see Computational Details). Cell parameters and bond distances for the optimized structure are in good agreement with the experimental data found for the LS state (Table 1). The optimized HS cell parameters are around 0.3 Å larger than the LS ones due to the elongation of Fe–L bond distances upon LS→HS spin transition. We have considered two possible coordination modes of the SO$_2$ molecule (see Scheme 1): one is shown in struture I with the sulfur atom coordinated to one platinum atom while a second one with the two oxygen atoms of one SO$_2$ molecule coordinated to two platinum atoms of

Table 1. Optimized Lattice Parameters (in Å and deg) and Bond Distances Involving the Transition Metal Atom Optimized Structures of the High- and Low-Spin of Clathrate {Fe(pz)[Pt(CN)$_4$]}·1SO$_2$[a]

	a	b	c	α	β	γ	d(Fe−NC)	d(Fe−Npz)	d(Pt−CN)
opt HS	7.507	7.362	7.091	88.2	90.4	90.0	2.099	2.141	1.980
opt LS	7.249	7.082	6.756	89.1	89.7	90.0	1.985	1.964	1.902
exp LS	7.162	7.162	6.749	90.0	90.0	90.0	1.924	1.984	1.987

[a]Using the Siesta code with the PBEsol functional and a numerical double-ζ basis set and pseudopotentials. Available experimental values of low-spin state are provided for comparison.

Scheme 1. Coordination Modes of the SO$_2$ Molecule Considered in the DFT Calculations: Planar (Left), O,O-Bridging (Middle), and Pyramidal (See Text)
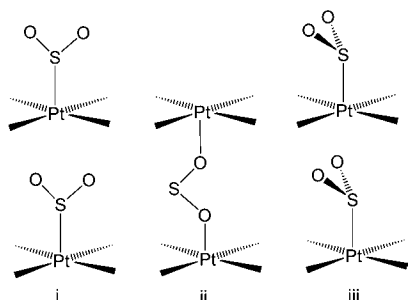
different layers acting as bridging ligands (see structure II). This second coordination mode was considered because each molecule can create two Pt−O bonds with the host in contrast with the first mode with only one Pt−S bond. The first coordination appears more stable than the second one, in agreement with the X-ray data. The relative position of SO$_2$ plane in the optimized structures to the layer surface is not perpendicular as found in the X-ray diffraction (see structure III). Nevertheless, in the optimized structure the SO$_2$ molecule adopts a pyramidal coordination geometry in which the iron, sulfur, and the two oxygen atoms are not in the same plane[7] in contrast to the inferred from the X-ray data. In order to clarify this point, we have performed a search of systems containing Pt−SO$_2$ bonds in the Cambridge Structural Database.[19] All of the nine CSD hits found[20] show a tilted structure as found in the optimized structure. Furthermore, calculations suggest that the tilted form is significantly more stable than the

perpendicular coordination for both spin states (10.7 and 14.0 kcal/mol for HS and LS states, respectively); hence, the X-ray data should correspond to an average or disordered structure. The calculated HS−LS energy gap that resulted was slightly larger for the SO$_2$ clathrate (26.8 kcal/mol) than for the guest-free compound (24.7 kcal/mol). Furthermore, the interaction energy with the SO$_2$ is −20.94 kcal/mol for the HS state while it is −22.52 kcal/mol for the LS state. These data justify the experimentally observed upward shift of the critical temperatures.

Host−guest interactions for HS and LS states were analyzed in terms of crystal orbital displacement (COD) curves.[21,22] In this representation, the projected density of states (PDOS) of the host or guest is subtracted from the interacting system PDOS at a given energy; in this way, only orbitals that change their energy upon interaction will appear on the curve, because contributions to PDOS from noninteracting orbitals will cancel. The integral of the COD curve with respect to energy (ICOD) contains information about the stabilization/destabilization of orbitals (negative sign means destabilization and positive sign stabilization), and at the Fermi level, it informs about charge transfer between subsystems. It is also possible to construct COD curves for the contribution of a selected group of basis functions to the PDOS.

COD curves for the complete SO$_2$ molecule and for the d-orbitals of Pt were constructed (Figure S4, Supporting Information). The most important changes due to the host⋯guest interactions are those that appear between −6 and −9 eV (Figure S5, Supporting Information). In the SO$_2$ PDOS, this energy range corresponds to the HOMO level and in the case of Pt to the d$_{z^2}$ orbital. The antibonding mixture of such orbitals corresponds to the DOS peak around −6 eV with only Pt and
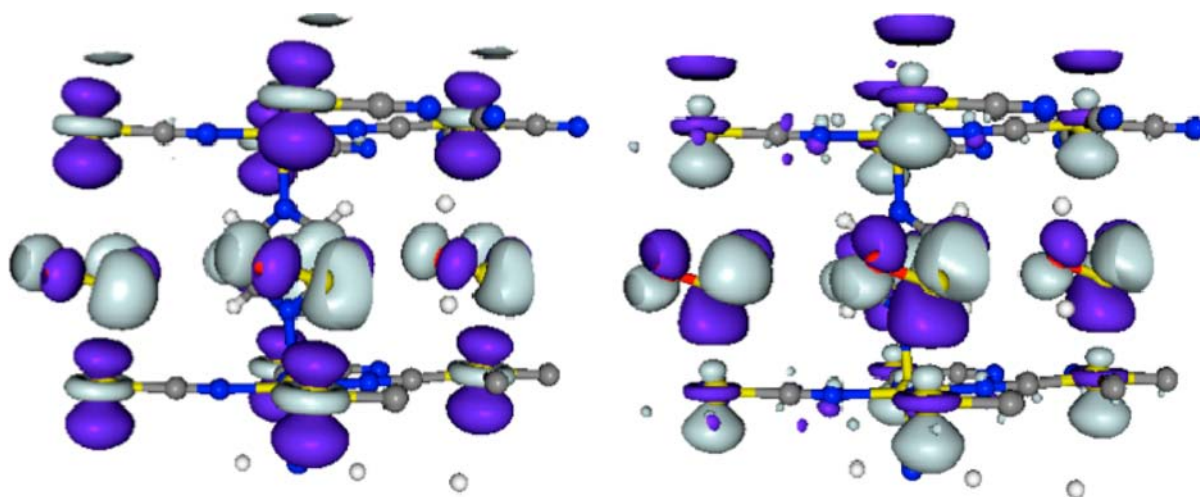
Figure 5. Representation of the orbitals involved in the Pt−SO$_2$ interactions for the HS state, (left) mixing between the SO$_2$ σ HOMO and the Pt-d$_{z^2}$, and (right) π-back-donation from the Pt-d$_{z^2}$−p$_z$ orbital to SO$_2$ π* LUMO.

SO_2 contribution that does not appear in the isolated host and guest plot. The corresponding bonding levels can be identified in the COD/ICOD plot as double positive−negative peaks around −8 eV. The negative ICOD value for these SO_2 levels is proof of the destabilization of such orbitals while the opposite sign is found for the Pt levels that are stabilized for such interaction. Thus, this interaction can be described as the mixing of the σ HOMO of the SO_2 molecule with the Pt-d_{z^2} orbital (Figure 5, left). The second main interaction corresponds to the π back-donation from the hybridized Pt-d_{z^2}−p_z orbital to the π^* LUMO of the SO_2 molecule (Figure 5, right) that in the DOS-COD diagrams appears slightly over −5 eV. Due to such interaction, the original SO_2 LUMO peak for the isolated molecule is destabilized for the mixing with the Pt-d_{z^2} orbital (Figures S4 and S5, Supporting Information.). The comparison of these results with those obtained when the SO_2 molecule is perpendicular to the layer indicates the following:[7] (i) Both coordination modes involve similar orbitals for the interaction involving SO_2 σ HOMO with the Pt-d_{z^2} orbital. (ii) However, in the perpendicular orientation the π-back-donation involves the Pt-d_{xz} or -d_{yz} orbitals[7] instead of the hybridized Pt-d_{z^2} orbital when the SO_2 is tilted.

It was shown in a previous work that the bridging pz rings perform a 4-fold jump motion about the coordinating nitrogen axis in the HS state. However, this motion is markedly reduced when the system is switched to the LS state, or almost stopped when it incorporates guest molecules (i.e., benzene).[14f] In the present case, although no significant interactions are observed between the SO_2 molecule and the pz ligand, the presence of SO_2 together with the smaller size of the unit cell in the LS state partially hinder the rotation of the pz (increase of the rotation barrier around 2 kcal/mol), and the minimum corresponding to a rotation angle of 90° becomes less stable than the orientation with 0° (Figure 6). For the HS state, the minimum to a rotation angle of 90° disappears after the inclusion of the SO_2 molecules, and the barrier also slightly increases.
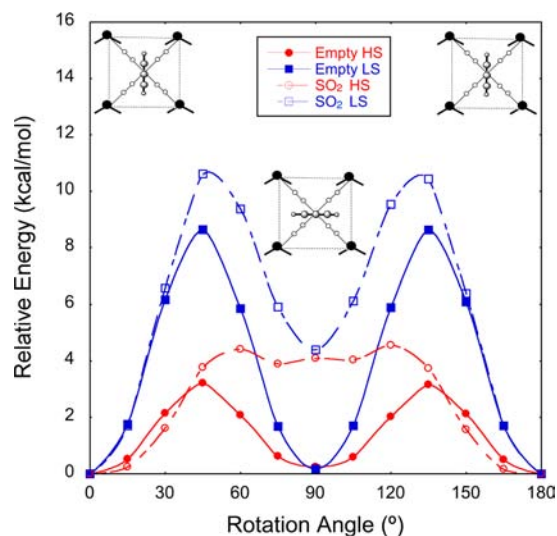

Figure 6. Dependence of the calculated energy with the rotation of the pyrazine ligand.

CONCLUSION

In summary, here we have demonstrated that the porous coordination polymer $\{Fe(pz)[Pt(CN)_4]\}$ (**1·1SO$_2$**) reversibly chemisorbs SO_2 at room temperature. This process occurs with a drastic change of electronic state of the Fe^{II} ion easily detectable by color change and magnetic properties. Consistent with the DFT calculations, the adsorption involves coordination of SO_2 to the Pt^{II} ion of the $[Pt(CN)_4]^{2-}$ moiety giving a square-pyramid coordination $[PtC_4S]$ with labile Pt−S bond and stabilization of the low-spin state of the Fe^{II} ion. The SO_2 uptake is higher than the values obtained for BPL-activated carbon or mixed metallic oxides, and most investigated MOFs based on carboxylate donor sites. The reversibility of the process offers an interesting opportunity for the efficient capture and release of SO_2.

EXPERIMENTAL SECTION

Materials and Sample Preparation. All manipulations were performed under argon atmosphere at room temperature with reagent grade solvents. All chemicals were purchased from commercial sources and used as received. The synthesis and characterization of $\{Fe(pz)[M^{II}(CN)_4]\}$ (M^{II} = Ni, Pd, Pt) was carried out as previously described (see for example ref 14b).

Physical Methods. Variable-temperature magnetic susceptibility measurements of **1·SO$_2$** (20−30 mg) were recorded at the rate of 2 K/min with a Quantum Design MPMS2 SQUID susceptometer operating at 1 T in the temperature interval 250−340 K. Experimental susceptibilities were corrected for diamagnetism of the constituent atoms by the use of Pascal's constants. Thermogravimetry (TG) measurements were performed on a Mettler Toledo TGA/SDTA 851e instrument in the 300−700 K temperature range in nitrogen atmosphere with a rate of 10 K/min. Adsorption isotherms of SO_2 were measured with BELSORP-max (BEL JAPAN Inc.). Single-crystal X-ray data of **1·nSO$_2$** were collected at 120 K on a Nonius Kappa-CCD single crystal diffractometer using graphite monochromated Mo Kα radiation (λ = 0.710 73 Å). A multiscan absorption correction was performed. The structure was solved by direct methods using SHELXS-97 and refined by full-matrix least-squares on F^2 using SHELXL-97.[23] The crystallographic data concerning compound **1·nSO$_2$** are gathered in Table 2.

Table 2. Crystal Data of Compound 1·nSO$_2$

empirical formula	$C_8H_8N_6O_{0.5}S_{0.25}Fe$
M_r	455.16
cryst syst	tetragonal
space group	$P4/mmm$
a (Å)	7.1620(2)
c (Å)	6.7490(4)
V (Å^3)	346.18(2)
Z	1
D_c (mg cm^{-3})	2.183
$F(000)$	210
μ (Mo Kα) (mm^{-1})	11.166
cryst size (mm^3)	0.04 × 0.06 × 0.06
T (K)	120(1)
no. total reflns	394
no. reflns [$I > 2\sigma(I)$]	392
$R_1{}^a$ [$I > 2\sigma(I)$]	0.0287
R_1 (all data)	0.0288
S	1.120

$^a R_1 = \Sigma||F_o| - |F_c||/\Sigma|F_o|$; $wR = [\Sigma[w(F_o{}^2 - F_c{}^2)^2]/\Sigma[w(F_o{}^2)^2]]^{1/2}$. $w = 1/[\sigma^2(F_o{}^2) + (mP)^2 + nP]$ where $P = (F_o{}^2 + 2F_c{}^2)/3$; $m = 0.0380$, $n = 0.0635$.

Computational Details. Full optimization of the low- and high-spin states of the $\{Fe(pz)[M^{II}(CN)_4]\}\cdot 1SO_2$ compound was performed by means of density functional theory[24] calculations using the Siesta code.[16] For such calculations, the PBEsol functional[17] was employed because it provides a better agreement with the available experimental crystal structure than other functionals, such as PBE.[25] Only valence electrons are included in the calculations, with the core being replaced by norm-conserving scalar relativistic pseudopotentials factorized in the Kleinman–Bylander form.[18a] The pseudopotentials are generated according to the method proposed by Trouiller and Martins.[18b] The following cutoff radii for the s, p, d, and f shells were used: Pt ($6s^1$ $r = 2.32$, $6p^0$ $r = 2.47$, $5d^9$ $r = 1.23$, $5f^0$ $r = 2.32$), Fe ($3s^2$ $r = 1.54$, $3p^6$ $r = 2.05$, $3d^6$ $r = 1.64$, $4f^0$ $r = 2.05$), S ($3s^2$ $r = 1.69$, $3p^4$ $r = 1.69$, $3d^0$ $r = 1.69$, $4f^0$ $r = 1.69$), O ($2s^2$ $r = 1.14$, $2p^3$ $r = 1.14$, $3d^0$ $r = 1.14$, $4f^0$ $r = 1.14$), N ($2s^2$ $r = 1.14$, $2p^3$ $r = 1.14$, $3d^0$ $r = 1.14$, $4f^0$ $r = 1.14$), C ($2s^2$ $r = 1.25$, $2p^2$ $r = 1.25$, $3d^0$ $r = 1.25$, $4f^0$ $r = 1.25$), and H ($1s^1$ $r = 1.14$, $2p^0$ $r = 1.14$, $3d^0$ $r = 1.14$, $4f^0$ $r = 1.14$). As basis set, a double-ζ with polarization was employed for the S, O, N, C, and H while for Pt atoms there was a double-ζ for the 6s and 5d orbitals and single-ζ for the 6p ones. For the iron atoms, there was single-ζ quality for the 3s, 3p, and 4p orbitals and double-ζ quality for the 3d and 4s ones. There are two parameters that control the accuracy of the numerical calculations: (i) since the wave function vanishes at the chosen confinement radius r_c, whose value is different for each atomic orbital, the energy radii of different orbitals is determined by a single parameter, the energy shift, which is the energy increase of the atomic eigenstate due to the confinement, and (ii) the integrals of the self-consistent terms are obtained with the help of a regular real space grid in which the electron density is projected. The grid spacing is determined by the maximum kinetic energy of the plane waves that can be represented in that grid. We have employed in the calculations an energy shift of 50 meV and maximum kinetic energy value of 250 Ry.

ASSOCIATED CONTENT

ⓢ Supporting Information

Experimental setup used to load microcrystalline samples with SO_2 (Figure S1), adsorption–desorption isotherms of SO_2 for $\{Fe(pz)[M^{II}(CN)_4]\}$ (M^{II} = Ni, Pd) at 293 and at 258 K (Figure S2), complete structure of **1·1SO₂** showing all possible positions of the atoms generated by symmetry (Figure S3), density of states of the low- and high-spin states of **1·1SO₂**, projected DOS and COD (integrated COD–ICOD) curves for Pt atoms of the host lattice (Figure S4), and SO_2 molecule for the low- and high-spin states of the **1·1SO₂** clathrate (Figure S5). Crystallographic data in CIF format. This material is available free of charge via the Internet at http://pubs.acs.org.

AUTHOR INFORMATION

Corresponding Author
*E-mail: jose.a.real@uv.es.

Notes
The authors declare no competing financial interest.

ACKNOWLEDGMENTS

REFERENCES

(1) See for example: (a) Lelieveld, J.; Heintzenberg, J. *Science* **1992**, *258*, 117. (b) Charlson, R. J.; Lovelock, J. E.; Andreae, M. O.; Warren, S. G. *Nature* **1987**, *326*, 655. (c) Capaldo, K.; Corbett, J. J.; Kasibhatia, P.; Fischbeck, P.; Pandis, S. N. *Nature* **1999**, *400*, 743. (d) Charlson, R. J. In *The Changing Atmosphere*; Rowland, F. S., Isaksen, I. S. A., Eds.; Wiley: Chichester, U.K., 1988; p 79. (e) Andreae, M. O. In *The Biogeochemical Cycling of Sulfur and Nitrogen in the Remote Atmosphere*; Galloway, J. N., Charlson, R. J., Andreae, M. O., Rohde, H., Eds.; Reidel: Dordrecht, 1985; p 5. (f) Brimblecombe, P.; Hammer, C.; Rohde, H.; Ryaboshapko, A.; Boutron, C. F. In *Evolution of the Global Biogeochemical Sulphur Cycle*; Brimblecombe, P., Lein, A. Y., Eds.; Wiley: New York, 1989; p 77.

(2) Usher, C. R.; Michel, A. E.; Grassian, V. H. *Chem. Rev.* **2003**, *103*, 4883.

(3) See for example: (a) Moreno-Castilla, C.; Carrasco-Marín, F.; Utrera-Hidalgo, E.; Rivera-Utrilla, J. *Langmuir* **1993**, *9*, 1378. (b) Zhang, P.; Wanko, H.; Ulrich, J. *Chem. Eng. Technol.* **2007**, *30*, 635. (c) Davini, P. *Carbon* **1990**, *28*, 565. (d) Gaur, V.; Sharma, A.; Verma, N. *Can. J. Chem. Eng.* **2007**, *85*, 188.

(4) (a) Gollakota, S. V.; Chriswell, C. D. *Ind. Eng. Chem. Res.* **1988**, *27*, 139. (b) Srinivasan, A.; Grutzeck, M. W. *Environ. Sci. Technol.* **1999**, *33*, 1464. (c) Kirik, S. D.; Dubkov, A. A.; Dubkova, S. A.; Sharonova, O. M.; Anshits, A. G. *Zeolites* **1992**, *12*, 292. (d) Kirschhock, C. E. A.; Sultana, A.; Godard, E.; Martens, J. A. *Angew. Chem., Int. Ed.* **2004**, *43*, 3722−3724.

(5) (a) Guimon, C.; Gervasini, A.; Auroux, A. *J. Phys. Chem. B* **2001**, *105*, 10316. (b) Baltrusaitis, J.; Cwiertny, D. M.; Grassian, V. H. *Phys. Chem. Phys.* **2007**, *9*, 5542. (c) Glover, T. G.; Sabo, D.; Vaughan, L. A.; Rossin, J. A.; Zhang, Z. J. *Langmuir* **2012**, *28*, 5695.

(6) (a) Albrecht, M.; van Koten, G. *Adv. Mater.* **1999**, *11*, 171. (b) Albrecht, M.; Gossage, R. A.; Lutz, M.; Spek, A. L.; van Koten, G. *Chem.—Eur. J.* **2000**, *6*, 1431. (c) Albrecht, M.; Lutz, M.; Spek, A. L.; van Koten, G. *Nature* **2000**, *406*, 970.

(7) Haase, J. *J. Phys.: Condens. Matter* **1997**, *9*, 3647.

(8) Kitagawa, S.; Kitaura, R.; Noro, S. *Angew. Chem., Int. Ed.* **2004**, *43*, 2334.

(9) (a) Morris, R. E.; Wheatley, P. S. *Angew. Chem., Int. Ed.* **2008**, *47*, 4966. (b) Li, J. R.; Kuppler, R. J.; Zhou, H. C. *Chem. Soc. Rev.* **2009**, *38*, 1477.

(10) Thallapally, P. K.; Motkuri, R. K.; Fernandez, C. A.; McGrail, B. P.; Behrooz, G. S. *Inorg. Chem.* **2010**, *49*, 4909.

(11) (a) Glover, G.; Peterson, G. W.; Schindler, B. J.; Britt, D.; Yaghi, O. *Chem. Eng. Sci.* **2011**, *66*, 163. (b) Britt, B.; Tranchemontagne, D.; Yaghi, O. M. *Proc. Natl. Acad. Sci. U.S.A.* **2008**, *105*, 11623.

(12) Yang, S.; Sun, J.; Ramirez-Cuesta, A. J.; Callear, S. K.; David, W. I. F.; Anderson, D. P.; Newby, R.; Blake, A. J.; Parker, J. E.; Tang, C. C.; Schröder, M. *Nat. Chem.* **2012**, *4*, 887.

(13) (a) Hofmann, K. A.; Küspert, F. Z. Z. *Anorg. Allg. Chem.* **1897**, *15*, 204. (b) Powell, H. M.; Rayner, J. H. *Nature (London)* **1949**, *163*, 566. (c) Rayner, J. H.; Powell, H. M. *J. Chem. Soc.* **1952**, 319. (d) Rayner, J. H.; Powell, H. M. *J. Chem. Soc.* **1958**, 3412. (e) Iwamoto, T. In *Inclusion Compounds*; Atwood, J. L., Davies, J. E.-D., MacNichol, D. D., Eds.; Academic: London, 1984; Vol. *1*, Chapter 2, p 29. (e) Iwamoto, T. In *Inclusion Compounds*; Atwood, J. L., Davies, J. E.-D., MacNichol, D. D., Eds.; Oxford University Press: London; Vol *5*, Chapter 6, p 177.

(14) (a) Niel, V.; Martinez-Agudo, J. M.; Muñoz, M. C.; Gaspar, A. B.; Real, J. A. *Inorg. Chem.* **2001**, *40*, 3838. (b) Ohba, M.; Yoneda, K.; Agustí, G.; Muñoz, M. C.; Gaspar, A. B.; Real, J. A.; Yamasaki, M.; Ando, H.; Nakao, Y.; Sakaki, S.; Kitagawa, S. *Angew. Chem., Int. Ed.* **2009**, *48*, 4767. (c) Agustí, G.; Ohtani, R.; Yoneda, K.; Gaspar, A. B.; Ohba, M.; Sánchez-Royo, J. F.; Muñoz, M. C.; Kitagawa, S.; Real, J. A. *Angew. Chem., Int. Ed.* **2009**, *48*, 8944. (d) Southon, P. D.; Liu, L.;

Fellows, E. A.; Price, D. J.; Halder, G. J.; Chapman, K. W.; Moubaraki, B.; Murray, K. S.; Létard, J. F.; Kepert, C. J. *J. Am. Chem. Soc.* **2009**, *131*, 10998. (e) Ohtani, R.; Yoneda, K.; Furukawa, S.; Horike, N.; Kitagawa, S.; Gaspar, A. B.; Muñoz, M. C.; Real, J. A.; Ohba, M. *J. Am. Chem. Soc.* **2011**, *133*, 8600. (f) Rodríguez-Velamazán, J. A.; González, M. A.; Real, J. A.; Castro, M.; Muñoz, M. C.; Gaspar, A. B.; Ohtani, R.; Ohba, M.; Yoneda, K.; Hijikata, Y.; Yanai, N.; Mizuno, M.; Ando, H.; Kitagawa, S. *J. Am. Chem. Soc.* **2012**, *134*, 5083.

(15) Spek, A. L. *PLATON, A Multipurpose Crystallographic Tool*; Utrecht University: Utrecht, The Netherlands, 2010.

(16) (a) Soler, J. M.; Artacho, E.; Gale, J. D.; García, A.; Junquera, J.; Ordejón, P.; Sánchez-Portal, D. *J. Phys.: Condens. Matter* **2002**, *14*, 2745. (b) Sánchez-Portal, D.; Ordejón, P.; Artacho, E.; Soler, J. M. *Int. J. Quantum Chem.* **1997**, *65*, 453.

(17) Perdew, J. P.; Ruzsinszky, A.; Csonka, G. I.; Vydrov, O. A.; Scuseria, G. E.; Constantin, L. A.; Zhou, X.; Burke, K. *Phys. Rev. Lett.* **2008**, *100*, 136406.

(18) (a) Kleinman, L.; Bylander, D. M. *Phys. Rev. Lett.* **1982**, *48*, 1425. (b) Trouiller, N.; Martins, J. L. *Phys. Rev. B* **1991**, *43*, 1993.

(19) Allen, F. H. *Acta Crystallogr., Sect. B* **2002**, *58*, 380.

(20) (a) Moody, D. C.; Ryan, R. R. *Inorg. Chem.* **1976**, *15*, 1823. (b) Ritchey, J. M.; Moody, D. C.; Ryan, R. R. *Inorg. Chem.* **1983**, *22*, 2276. (c) Terheijden, J.; van Koten, G.; Mul, W. P.; Stufkens, D. J.; Muller, F.; Stam, C. H. *Organometallics* **1986**, *5*, 519. (d) Albrecht, M.; Lutz, M.; Schreurs, A. M. M.; Lutz, E. T. H.; Spek, A. L.; van Koten, G. *J. Chem. Soc., Dalton Trans.* **2000**, 3797. (e) Albrecht, M.; Gossage, R. A.; Spek, A. L.; van Koten, G. *Chem. Commun.* **1998**, 1003. (f) Albrecht, M.; Gossage, R. A.; Lutz, M.; Spek, A. L.; van Koten, G. *Chem.—Eur. J.* **2000**, *6*, 1431. (g) Eller, P. G.; Ryan, R. R.; Moody, D. C. *Inorg. Chem.* **1976**, *15*, 2442. (h) Steenwinkel, P.; Kooijman, H.; Smeets, W. J. J.; Spek, A. L.; Grove, D. M.; van Koten, G. *Organometallics* **1998**, *17*, 5411.

(21) Ruiz, E.; Alvarez, S.; Hoffmann, R.; Bernstein, J. *J. Am. Chem. Soc.* **1994**, *116*, 8207.

(22) Muñoz-Lara, F. J.; Gaspar, A. B.; Aravena, D.; Ruiz, E.; Muñoz, M. C.; Ohba, M.; Ohtani, R.; Kitagawa, S.; Real, J. A. *Chem. Commun.* **2012**, *48*, 4686.

(23) Sheldrick, G. M. *Acta Crystallogr., Sect. A* **2008**, *64*, 112.

(24) Martin, R. M. *Electronic Structure, Basic Theory and Practical Methods*; Cambridge University Press: Cambridge, U.K., 2004.

(25) Perdew, J.; Burke, K.; Ernzerhof, M. *Phys. Rev. Lett.* **1996**, *77*, 3865.